Bulk and surface spin-flop transitions in an antiferromagnetic *XYZ* chain

J. Karadamoglou* and N. Papanicolaou†
Department of Physics, University of Crete, and Research Center of Crete, Heraklion, Greece
(Received 29 April 1999)

Spin-flop transitions are studied within a spin-$\frac{1}{2}$ antiferromagnetic *XYZ* chain immersed in a uniform bias magnetic field. For a special choice of anisotropy the bulk spin-flop transition occurs at a critical field H_b characterized by the onset of ''accidental'' degeneracy in the energy spectrum that may indicate a hidden symmetry. On an open chain the bulk transition is preceded by a surface spin-flop transition induced by a surface magnon that turns soft at a new critical field $H_s<H_b$, while an antiferromagnetic domain wall is realized in the ground state as the bias field approaches H_b. These $T=0$ phase transitions could be observed through electron-spin resonance on magnetic chains doped with nonmagnetic ions. [S0163-1829(99)01137-6]

I. INTRODUCTION

Surface effects that could be observed in an antiferromagnet were theoretically predicted some time ago.[1–3] However, the subject was revived only recently with the experimental observation of a surface spin-flop transition in an Fe/Cr multilayer.[4–6] The precise nature of the transition proved to be more intricate than originally envisaged but has been clarified in a number of recent theoretical investigations.[7–17] The advantage of a multilayer is that it can be modeled by a classical spin chain characterized by an isotropic exchange interaction and a single-ion quadratic anisotropy.

In view of this development we return to the problem of crystalline antiferromagnets which are more appropriately described by quantum spin systems. Specifically, we intend to study spin-flop transitions for a spin-$\frac{1}{2}$ *XYZ* model whose Hamiltonian

$$W=\sum_{l=1}^{\Lambda-1}\left(J_1S_l^xS_{l+1}^x+J_2S_l^yS_{l+1}^y+J_3S_l^zS_{l+1}^z\right)-H\sum_{l=1}^{\Lambda}S_l^z \tag{1.1}$$

is defined on an open chain with Λ sites. Various quasi-one-dimensional magnets that are thought to be approximated by special cases of Eq. (1.1) have already been identified. Furthermore a statistically significant sample of free boundaries may be experimentally accessible[18] through doping with nonmagnetic ions which creates within the crystal open magnetic chains of varying length. Therefore, a theoretical study of surface effects is now more meaningful than ever.

In fact, the *XYZ* model has been the subject of an immense amount of theoretical work based on the Bethe ansatz[19] or any of its variants. In particular, recent activity has concentrated on surface effects in the presense of boundary fields or other integrable impurities.[20] However, the model is not known to be completely integrable in the presense of the uniform bulk field H in Eq. (1.1), except in special limits such as the U(1)-symmetric *XXZ* model ($J_1=J_2$) in a field directed along the symmetry axis. Hence, the present work will proceed by a more direct analytical approach supported by numerical diagonalization.

Hamiltonian (1.1) is here restricted by the inequalities

$$|J_1|\leqslant J_2<J_3 \tag{1.2}$$

and thus describes an antiferromagnetic chain in a field pointing along the easy axis. To set the stage for the study of the quantum model we have carried out a classical calculation[21] which revealed the existence of a surface spin-flop transition analogous to that encountered in multilayers. A peculiarity of the classical ground state is its independence on the specific value of J_1, in the range $|J_1|\leqslant J_2$, a property that is not sustained in the quantum model. But the recent work of Kyriakidis and Loss[22] on an unrelated subject (Bloch oscillations) suggested to us that the most classical antiferromagnet is obtained by the special choice of the exchange constants

$$-J_1=J_2\equiv 1,\quad J_3\equiv\Delta>1, \tag{1.3}$$

which is consistent with inequalities (1.2). If u and d denote spin-up and spin-down states, the two fully polarized Néel states

$$|N_A\rangle=|d,u,d,u,\ldots\rangle,\quad |N_B\rangle=|u,d,u,d,\ldots\rangle \tag{1.4}$$

are then the two (degenerate) exact ground states when the applied field is sufficiently weak.

Some special features of model (1.3) become apparent by performing the familiar canonical transformation

$$S_l^x=T_l^x,\quad S_l^y=(-1)^lT_l^y,\quad S_l^z=(-1)^lT_l^z, \tag{1.5}$$

where the ''pseudospin'' variables $\mathbf{T}_l$ again satisfy the standard spin commutation relations and map the Hamiltonian to

$$W=-\sum_{l=1}^{\Lambda-1}\left[T_l^xT_{l+1}^x+T_l^yT_{l+1}^y+\Delta\left(T_l^zT_{l+1}^z-\frac{1}{4}\right)\right]-H\sum_{l=1}^{\Lambda}(-1)^lT_l^z, \tag{1.6}$$

which describes an easy-axis ''ferromagnet'' in a staggered magnetic field. In Eq. (1.6) we have included a trivial additive constant to provide a convenient normalization for the energy eigenvalues.

It is clear from Eq. (1.6) that the model (1.3) is also endowed with a U(1) symmetry because the total azimuthal pseudospin

$$\tau=\sum_{l=1}^{\Lambda} T_l^z=\sum_{l=1}^{\Lambda} (-1)^l S_l^z \tag{1.7}$$

obviously commutes with the Hamiltonian and thus the Hilbert space breaks up into $\Lambda+1$ sectors characterized by the good quantum number $\tau=\Lambda/2-\lambda$ with $\lambda=0,1,\ldots,\Lambda$. Although this observation will greatly simplify calculations, the quantum number τ is not related to a simple physical observable. Instead we shall be interested in the total azimuthal magnetization

$$M=\sum_{l=1}^{\Lambda} S_l^z=\sum_{l=1}^{\Lambda} (-1)^l T_l^z, \tag{1.8}$$

which does not commute with the Hamiltonian and its expected values cannot be predicted by simple quantization. One of our objectives in the following is to determine the ground-state expectation value $M=M(\Delta,H)$ as a function of anisotropy Δ and applied field H.

Significant analytical progress can be made for the specific choice (1.3) which will serve as a prototype for further consideration of the full range of models defined by inequalities (1.2). In Sec. II we provide a complete calculation of one-magnon excitations with or without open boundaries. These results already suggest the occurrence of a bulk spin-flop (BSF) transition at a critical field H_b, which is preceded by a surface spin-flop (SSF) transition at a critical field $H_s<H_b$ in the presence of open boundaries. The two types of transition are analyzed in Secs. III and IV. Antiferromagnetic domain walls arise naturally in the description of the SSF transition and are thus also discussed in Sec. IV. In Sec. V we summarize some of our main conclusions, in addition to presenting some preliminary results for other quantum spin models in the range (1.2). For clarity of presentation we found it useful to restrict attention to an even chain ($\Lambda=2N$) in the main text, while the necessary modifications for the case on an odd chain ($\Lambda=2N+1$) are discussed in the Appendix.

II. BULK AND SURFACE MAGNONS

The eigenstates of the Hamiltonian (1.6) are linear superpositions of states of the form $|\tau_1,\tau_2,\ldots,\tau_\Lambda\rangle$ where the τ_l's take the values 1/2 or $-1/2$ in any combination that preserves their sum τ. The Néel states (1.4) are mapped to two completely polarized ''ferromagnetic'' states, with $\tau=\pm\Lambda/2$, which are exact eigenstates, with energy $E=0$, for any value of the applied field. It is also clear that these are the two degenerate ground states at vanishing field. The first question is then to determine the field region over which the polarized states persist as the ground states of the system.

One is thus lead to study excitations, the simplest possibilities being one-magnon modes with $\tau=\Lambda/2-1$ or $-\Lambda/2+1$. It is sufficient to consider only the former case, information about the latter being inferred by extending the field region to both positive and negative values of H. The one-magnon eigenvalue problem reads

$$W|\psi\rangle=E|\psi\rangle, \quad |\psi\rangle=\sum_{l=1}^{\Lambda} C_l|l\rangle, \tag{2.1}$$

where we have simplified the notation by asserting that $|l\rangle$ is the state where $\tau_l=-1/2$ but all other τ's are equal to 1/2. An explicit form of the eigenvalue equations is then given by

$$\begin{aligned}
&(\Delta/2-H-E)C_1=\frac{1}{2}C_2,\\
&[\Delta+(-1)^l H-E]C_l=\frac{1}{2}(C_{l+1}+C_{l-1}),\\
&\qquad\qquad l=2,3,\ldots,\Lambda-1,\\
&(\Delta/2+H-E)C_\Lambda=\frac{1}{2}C_{\Lambda-1},
\end{aligned} \tag{2.2}$$

and are valid on an open chain with Λ sites. Here and throughout the main text we assume that the chain is even ($\Lambda=2N$). We further introduce the sublattice variables

$$A_n=C_{2n-1}, \quad B_n=C_{2n}, \quad n=1,2,\ldots,N \tag{2.3}$$

in terms of which the linear system (2.2) reads

$$\begin{aligned}
&(\Delta/2-H-E)A_1=\frac{1}{2}B_1,\\
&(\Delta-H-E)A_n=\frac{1}{2}(B_{n-1}+B_n), \quad n=2,3,\ldots,N,\\
&(\Delta+H-E)B_n=\frac{1}{2}(A_n+A_{n+1}), \quad n=1,2,\ldots,N-1,\\
&(\Delta/2+H-E)B_N=\frac{1}{2}A_N.
\end{aligned} \tag{2.4}$$

It is instructive to consider in parallel a cyclic or periodic chain with the same number of sites, in order to establish a simple reference case which will enable us to better appreciate surface effects that may arise on an open chain. The first and fourth equations in Eq. (2.4) are absent on a cyclic chain, and the remaining two equations are valid for all $n=1,2,\ldots,N$. It is then a straightforward matter to eliminate B_n to obtain the equivalent system

$$\begin{aligned}
&B_n=\frac{1}{2}\frac{A_n+A_{n+1}}{\Delta+H-E},\\
&[(\Delta-E)^2-H^2]A_n=\frac{1}{4}(2A_n+A_{n+1}+A_{n-1}),
\end{aligned} \tag{2.5}$$

whose solution is $A_n=e^{ikn}$, where $k=2\pi\nu/N$ with $\nu=0,1,\ldots,N-1$ is a sublattice crystal momentum, provided that the energy is given by

$$E=\Delta\pm\sqrt{H^2+\cos^2(k/2)}. \tag{2.6}$$

Viewed as functions of the applied field the energy eigenvalues are contained within the two shaded regions of Fig. 1 and their distribution becomes increasingly dense in the bulk limit $N\to\infty$. The shaded regions are bounded from above and below by the two curves $E=\Delta\pm\sqrt{H^2+1}$ and display a

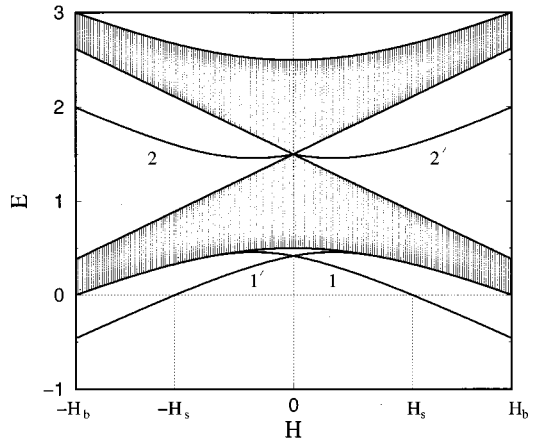

FIG. 1. Field dependence of the one-magnon spectrum for the specific anisotropy $\Delta=1.5$.

middle gap extended between the curves $E=\Delta\pm H$. The lowest gap closes ($E=0$) at $H=\pm H_b$ where

$$H_b=\sqrt{\Delta^2-1} \tag{2.7}$$

is a critical field of special importance in the following. The preceding derivation already indicates that the simple Néel states (1.4) can no longer be the ground states for field values outside the interval $[-H_b,H_b]$. Further analysis of the cyclic chain given in Sec. III will establish that H_b provides the critical boundary of the BSF transition.

We now return to the main theme and examine the possibility of one-magnon surface modes on an open chain. Solution of the linear system (2.4) is complicated by the appearance of the two distinct equations at the outer layers. However, the essential new ingredients can be obtained analytically on a semi-infinite chain. The fourth equation in Eq. (2.4) may then be ignored and the third may again be used to eliminate B_n as in Eq. (2.5). The first two equations are written as

$$\begin{aligned}(\Delta/2-H-E)(\Delta+H-E)A_1&=\frac{1}{4}(A_1+A_2),\\ [(\Delta-E)^2-H^2]A_n&=\frac{1}{4}(2A_n+A_{n+1}+A_{n-1}),\end{aligned} \tag{2.8}$$

where $n=2,3,\ldots,\infty$. A surface mode is described by a special solution of the form

$$A_n=\xi^n,\quad B_n=\frac{1}{2}\,\frac{1+\xi}{\Delta+H-E}\,\xi^n \tag{2.9}$$

supplemented by the requirement $|\xi|<1$ which guarantees that the state decay exponentially away from the boundary. Equations (2.8) reduce to

$$\begin{aligned}(\Delta/2-H-E)(\Delta+H-E)&=\frac{1}{4}(1+\xi),\\ (\Delta-E)^2-H^2&=\frac{1}{4}(2+\xi+1/\xi),\end{aligned} \tag{2.10}$$

and should be viewed as a system of two algebraic equations for the unknowns ξ and E. Detailed examination of the roots that satisfy the condition $|\xi|<1$ yields two distinct surface modes which we discuss in turn.

The most interesting surface mode is given by the root $\xi=\xi_1$ and $E=E_1$ with

$$\xi_1=\frac{1}{2\Delta^2}[\sqrt{(\Delta^2+4\Delta H-1)^2+4\Delta^2}-(\Delta^2+4\Delta H-1)],$$

$$E_1=\Delta-\sqrt{H^2+\frac{1}{4}(2+\xi_1+1/\xi_1)}, \tag{2.11}$$

and its energy labeled as curve 1 in Fig. 1 lies below the one-magnon continuum. This curve emanates from the continuum at the characteristic field $-H_0$ with

$$H_0=\frac{\Delta^2-1}{2\Delta} \tag{2.12}$$

and persists in the field region $H>-H_0$. The parameter ξ_1 is equal to unity at $-H_0$ but lies in the interval $0<\xi_1<1$ for $H>-H_0$. This surface state exists as a distinct gap mode below the continuum even at vanishing field ($H=0$) where $\xi_1=1/\Delta^2$ and $E_1=(\Delta^2-1)/2\Delta$.

A second root satisfying the condition $|\xi|<1$ is given by $\xi=\xi_2$ and $E=E_2$ with

$$\xi_2=-\frac{1}{2\Delta^2}[\sqrt{(\Delta^2+4\Delta H-1)^2+4\Delta^2}+(\Delta^2+4\Delta H-1)],$$

$$E_2=\begin{cases}\Delta-\sqrt{H^2+\frac{1}{4}(2+\xi_2+1/\xi_2)} & -H_0<H<0,\\ \Delta+\sqrt{H^2+\frac{1}{4}(2+\xi_2+1/\xi_2)} & H<-H_0.\end{cases} \tag{2.13}$$

The two branches in E_2 join smoothly at $-H_0$ and their union is labeled as curve 2 in Fig. 1. Therefore, the second root describes a surface mode with energy in the middle gap of the magnon continuum. The parameter ξ_2 lies in the interval $-1<\xi_2<0$ and thus the middle-gap mode decays away from the boundary in an oscillatory manner.

To complete the description of Fig. 1 we must now reconcile the preceding analytical results on a semi-infinite chain with those obtained by numerical diagonalization of the linear system (2.2) or (2.4) on a finite open chain. For any given $\Lambda=2N$ the majority of eigenvalues fall within the shaded regions of Fig. 1, but a finite number of eigenvalues occur outside the continuum for each field H. Also note that a dublication of gap modes should be expected on an open chain because surface states can now be formed near either one of the two free ends. Indeed, in addition to confirming the gap modes 1 and 2 predicted on a semi-infinite chain, the numerical diagonalization also yields the two mirror modes $1'$ and $2'$ shown in Fig. 1.

The energies of the gap modes calculated analytically on a semi-infinite chain with $\Delta=1.5$ agree with the numerical results to several significant figures for $\Lambda=10$ while the agreement improves rapidly with increasing Λ or Δ. Hence the numerical simulations described in Secs. III and IV for

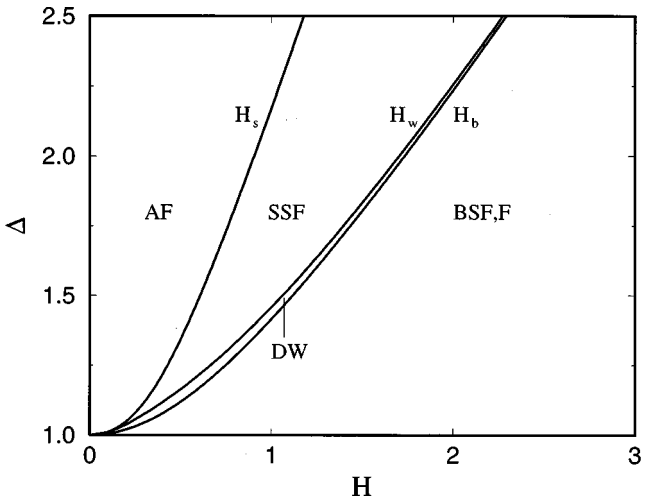

FIG. 2. The $T=0$ phase diagram for the quantum model (1.3). The bulk and surface critical boundaries H_b and H_s are given analytically by Eqs. (2.7) and (2.14), and the domain-wall boundary H_w was obtained numerically as described in Sec. IV.

chains of modest size are expected to provide a reliable picture for most values of Δ of practical interest.

The most important conclusion derived from the one-magnon calculation becomes apparent by simple inspection of Fig. 1. The surface modes in the lower gap are degenerate with the Néel states at the critical fields $\pm H_s$. The field H_s is computed from the condition $E_1=0$ where E_1 is given by Eq. (2.11). A straightforward calculation shows that

$$H_s=\frac{1}{4\Delta}[\sqrt{(\Delta^2-1)(9\Delta^2-1)}-(\Delta^2-1)]. \quad (2.14)$$

Outside the interval $[-H_s,H_s]$ the Néel states cease to be the lowest-energy states. Therefore, the BSF transition anticipated to occur at the critical field H_b of Eq. (2.7) is preceded on an open chain by a SSF transition at $H_s<H_b$. The critical fields H_s and H_b coincide with those found in the classical calculation[21] except for an overall factor of 2 which originates in the normalization of the classical spin to unity. The curves $H=H_s(\Delta)$ and $H=H_b(\Delta)$ provide the main critical boundaries in the $T=0$ phase diagram provisionally shown in Fig. 2 and further analyzed in Secs. III and IV.

The surface magnon that drives the SSF transition in the present quantum model is the analog of the Mills-Saslow mode[2] which was derived semiclassically in a model with single-ion anisotropy and played an important role in the theory of classical multilayers.[17] Interestingly, the currently calculated ratio H_b/H_s approaches the value $\sqrt{2}$ in the isotropic limit $\Delta\to 1^+$, in agreement with the corresponding ratio in the limit of vanishing single-ion anisotropy.[2] In the opposite limit, $\Delta\to\infty$, H_b/H_s approaches 2 which may also be deduced from an elementary analysis of the Ising chain.

III. BULK SPIN-FLOP TRANSITION

In this section we focus on a cyclic chain with an even number of sites and examine in greater detail the BSF transition at the critical field H_b of Eq. (2.7) suggested by the one-magnon calculation. In a curious turn of events, the recent work of Alcaraz, Salinas, and Wrezinski[23] on an open spin chain in the presence of suitable boundary fields proved to be very instructive for the current work on a cyclic chain in a bulk bias field H.

We may also invoke the cluster argument of Bader and Schilling[24] on a cyclic chain noting that the Hamiltonian may then be written as a sum of cell Hamiltonians, namely

$$W=\sum_{l=1}^{\Lambda} W_l,$$

$$W_l=-\left[T_l^xT_{l+1}^x+T_l^yT_{l+1}^y+\Delta\left(T_l^zT_{l+1}^z-\frac{1}{4}\right)\right]-\frac{1}{2}H(-1)^l(T_l^z-T_{l+1}^z), \quad (3.1)$$

and thus the ground-state energy E_0 satisfies the inequality

$$\frac{1}{2}\Lambda(E_++E_-)\leqslant E_0, \quad (3.2)$$

where $E_\pm$ are the ground-state energies of the two-spin Hamiltonians

$$W_\pm=-\left[T_1^xT_2^x+T_1^yT_2^y+\Delta\left(T_1^zT_2^z-\frac{1}{4}\right)\right]\pm\frac{1}{2}H(T_1^z-T_2^z). \quad (3.3)$$

The eigenvalues of both W_+ and W_- are given by

$$\frac{1}{2}(\Delta+\sqrt{H^2+1}),\ 0,\ 0,\ \frac{1}{2}(\Delta-\sqrt{H^2+1}), \quad (3.4)$$

where the first eigenvalue is always positive and the fourth one may be positive or negative depending on the field strength H. Therefore, inequality (3.2) is written as

$$\Lambda\min\left[0,\frac{1}{2}(\Delta-\sqrt{H^2+1})\right]\leqslant E_0\leqslant 0, \quad (3.5)$$

and has been supplemented by $E_0\leqslant 0$ which follows from the fact that the polarized states are eigenstates of the complete Hamiltonian with vanishing energy for any value of the applied field. An immediate consequence of Eq. (3.5) is that the true ground-state energy vanishes when $-H_b\leqslant H\leqslant H_b$, where H_b is precisely the critical field (2.7), and thus coincides with the energy of the polarized states.

The preceding result strengthens the conclusion that the BSF transition occurs at the critical field H_b but a more detailed argument is required to determine the precise nature of the transition. The work of Sec. II already established that the lowest-energy state in the one-magnon sector becomes degenerate with the polarized states at H_b. We shall further show that the lowest-energy states of all multimagnon sectors become degenerate at the same critical field, in analogy with a similar result in the model of Ref. 23. When $H=H_b$ it is convenient to introduce the parametrization

$$\Delta=\frac{1}{2}\left(q+\frac{1}{q}\right),\quad H=\frac{1}{2}\left(q-\frac{1}{q}\right), \quad (3.6)$$

where $\Delta>1$ and $q=\Delta+\sqrt{\Delta^2-1}>1$.

To motivate the demonstration we return to the one-magnon calculation and specifically consider the lowest-energy state at H_b obtained by setting $k=0$ and $E=0$ in Eqs. (2.5) and (2.6) to yield $A_n=1$ and $B_n=1/q$ for all $n=1,2,\ldots,N$. In the notation of Eq. (2.1) this special one-magnon state reads

$$C_l=q^{-1/2(-1)^l}, \tag{3.7}$$

where we have also included an overall normalization factor $\sqrt{q}$.

We next consider the two-magnon eigenvalue problem

$$W|\psi\rangle=E|\psi\rangle, \quad |\psi\rangle=\sum_{l_1<l_2} C(l_1,l_2)|l_1,l_2\rangle, \tag{3.8}$$

where $|l_1,l_2\rangle$ is a state with $\tau_{l_1}=-1/2=\tau_{l_2}$ and all other τ's equal to 1/2. On a cyclic chain the generic eigenvalue equation is

$$\begin{aligned}\{2\Delta+[(-1)^{l_1}+(-1)^{l_2}]H-E\}C(l_1,l_2)&\\ =\frac{1}{2}[C(l_1+1,l_2)+C(l_1-1,l_2)+C(l_1,l_2+1)&\\ +C(l_1,l_2-1)],&\end{aligned} \tag{3.9}$$

and should be completed with the meeting condition[19]

$$\Delta C(l,l+1)=\frac{1}{2}[C(l,l)+C(l+1,l+1)], \tag{3.10}$$

where one formally extends the definition of $C(l_1,l_2)$ to coinciding arguments ($l_1=l_2$) which are absent in Eq. (3.8). When Δ and H are given by Eq. (3.6) the wave function

$$C(l_1,l_2)=q^{-1/2[(-1)^{l_1}+(-1)^{l_2}]} \tag{3.11}$$

satisfies Eq. (3.9), with $E=0$, as well as the meeting condition (3.10). We have thus obtained a special two-magnon eigenstate which is degenerate with both the one-magnon state (3.7) and the completely polarized states at the critical field H_b.

These elementary results possess a simple generalization to an arbitrary sector. A set of exact eigenstates with vanishing energy is given by

$$|\psi_\tau\rangle=\sum_{\{\tau\}} q^{1/2\Sigma_{l=1}^{\Lambda}(-1)^l\tau_l}|\tau_1,\tau_2,\ldots,\tau_\Lambda\rangle, \tag{3.12}$$

where the sum extends over all configurations $\{\tau\}=(\tau_1,\tau_2,\ldots,\tau_\Lambda)$ which are consistent with a definite azimuthal pseudospin

$$\tau=\sum_{l=1}^{\Lambda}\tau_l=N,N-1,\ldots,-N, \tag{3.13}$$

where $\Lambda=2N$. As a check of consistency one may apply Eq. (3.12) for $\tau=N-1$ and $N-2$ to recover the one- and two-magnon wave functions (3.7) and (3.11). For other values of τ our basic result (3.12) can be established by a straightforward generalization of the two-magnon calculation given above.

A numerical calculation of all eigenstates and eigenvalues, for various $\Lambda\leqslant 12$, confirms that the ground states of all sectors become degenerate at the critical field. Excited states also exhibit some accidental degeneracy that cannot be accounted for by the U(1) symmetry. One is thus tempted to conclude that the model acquires a larger symmetry at the critical point; perhaps analogous to the quantum-group $U_q[\mathrm{SU}(2)]$ symmetry of the model with boundary fields studied in Refs. 23, 25. We shall not pause to examine the possibility of a hidden symmetry in the present model because the explicit result (3.12) proves to be sufficient to illuminate the nature of the BSF transition.

Thus the emerging qualitative picture is substantiated with an explicit calculation of the ground-state expectation value of the total magnetization M of Eq. (1.8) which vanishes in the region $H<H_b$ but acquires finite values for $H>H_b$. A sudden jump occurs at the critical field which can be calculated analytically on an even cyclic chain of any size. The calculation is based on the important observation that the $\tau=0$ sector prevails above H_b, in the sense that it contains the unique absolute ground state for $H>H_b$. The last statement is corroborated by numerical diagonalization on short chains of varying size. Therefore the magnetization jump at the critical field is given by

$$M=\sum_{l=1}^{\Lambda}(-1)^l\frac{\langle\psi_0|T_l^z|\psi_0\rangle}{\langle\psi_0|\psi_0\rangle}, \tag{3.14}$$

where $|\psi_0\rangle$ is the state (3.12) applied for $\tau=0$. The special structure of this state permits us to write

$$M=q\frac{\partial}{\partial q}\ln\langle\psi_0|\psi_0\rangle \tag{3.15}$$

and the problem reduces to the calculation of the norm $\langle\psi_0|\psi_0\rangle$. A reasonable amount of combinatorics leads to

$$\langle\psi_0|\psi_0\rangle=\sum_{\nu=0}^{N}\left[\frac{N!}{(N-\nu)!\,\nu!}\right]^2 q^{N-2\nu} \tag{3.16}$$

and

$$M=\frac{1}{\langle\psi_0|\psi_0\rangle}\sum_{\nu=0}^{N}(N-2\nu)\left[\frac{N!}{(N-\nu)!\,\nu!}\right]^2 q^{N-2\nu}. \tag{3.17}$$

It is also possible to provide an integral representation of the sums to obtain

$$\begin{aligned}\mu=\frac{M}{2N}=\frac{1}{2}\sqrt{\Delta^2-1}\frac{I_{N-1}}{I_N},&\\ I_N\equiv\frac{1}{\pi}\int_0^\pi(\Delta+\cos\theta)^N d\theta,&\end{aligned} \tag{3.18}$$

where μ is the average magnetization per site, a quantity that is more appropriate for the discussion of the thermodynamic limit.

Analytical calculation of the magnetization for $H>H_b$ is impossible at present because the $\tau=0$ ground state becomes increasingly complex away from the critical point. We have thus resorted to numerical diagonalization on short chains.

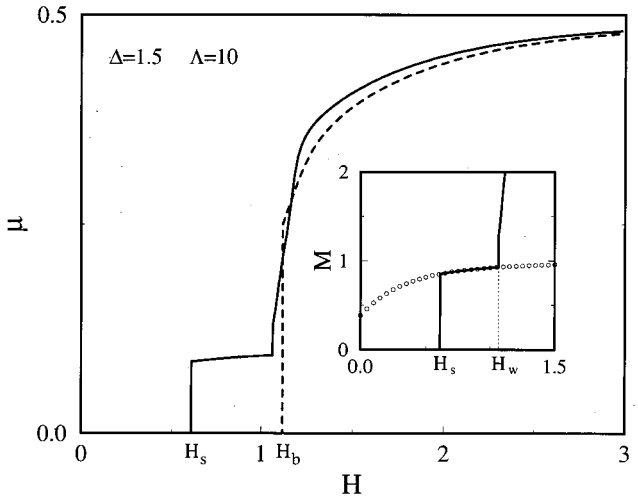

FIG. 3. Field dependence of the average magnetization per site $\mu = M/\Lambda$ in the ground state of a chain with $\Delta = 1.5$ and $\Lambda = 10$. The dashed line corresponds to a cyclic chain and the solid line to an open chain with the same number of sites. The inset focuses on the first step of the main figure and compares the total magnetization M to the analytical prediction (4.4) depicted by open circles.

Memory requirements restrict us to the range $\Lambda \leqslant 12$ if we wish to compute all eigenstates. However, we have been able to extend the range to $\Lambda \leqslant 22$ for the calculation of the ground-state energy via a Lanczos algorithm. The latter proved to be somewhat less reliable as well as time consuming in the calculation of the magnetization. Therefore, the Lanczos algorithm is used on chains with $\Lambda \leqslant 22$ for the investigation of those issues that depend exclusively on the ground-state energy. But results for the magnetization are limited to $\Lambda \leqslant 16$, using either complete diagonalization or the Lanczos algorithm, or both. In all cases we provide explicit estimates of finite-size effects which suggest that the derived overall picture is indeed reliable.

For instance, the average magnetization per site $\mu = M/\Lambda$ calculated on a cyclic chain with $\Delta = 1.5$ and $\Lambda = 10$ is depicted by a dashed line in Fig. 3 and exhibits a sudden jump at the critical field $H_b = 1.118\,033\,99$ given by Eq. (2.7). The size of the jump was found equal to $\mu = 0.249\,732\,68$, also in perfect agreement with the analytical result (3.18) applied for $\Delta = 1.5$ and $N = \Lambda/2 = 5$. Away from the critical point the magnetization increases smoothly to achieve the saturated ferromagnetic value $\mu = 1/2$ in the limit $H \to \infty$.

Although H_b is independent of chain size, the magnetization does depend on $\Lambda = 2N$ for $H \geqslant H_b$. A good estimate of its size dependence is obtained by taking advantage of the analytical result (3.18). In the limit $N \to \infty$ the integral is dominated by the maximum value of the integrand achieved at $\theta = 0$ to yield $I_N \sim (\Delta + 1)^N$ and

$$\mu = \lim_{N \to \infty} \left(\frac{M}{2N} \right) = \frac{1}{2} \sqrt{\frac{\Delta - 1}{\Delta + 1}}. \tag{3.19}$$

Applied for $\Delta = 1.5$ the above expression leads to $\mu = 0.223\,606\,80$ which is overestimated by the value at $\Lambda = 10$ quoted earlier by about 12%. More generally, the magnetization at the critical field computed on chains with $\Lambda \sim 10$ does not differ from its $\Lambda \to \infty$ limit by more than 13%, for all $\Delta > 1$, and the agreement improves at large Δ. It is also likely that the thermodynamic limit for $H > H_b$ could be reached by extrapolation, but this is clearly an issue of no special urgency at this point.

The analytical result (3.19) reveals yet another surprise, for it coincides with the magnetization obtained within the classical calculation[21] at the onset of the BSF phase which is described by a canted spin configuration. This curious fact could be investigated further by generalizing the special states (3.12) to arbitrary spin s, also in analogy with a similar calculation in the model of Ref. 23. One should then be able to explicitly study the classical (large-s) limit on any finite chain and eventually explain its coincidence with the quantum prediction (3.19) in the thermodynamic limit.

To summarize, the $T = 0$ phase diagram is rather simple on a cyclic chain and consists of a single boundary $H = H_b(\Delta)$ given by Eq. (2.7). To the left of this boundary the ground state is purely antiferromagnetic (AF) and to the right it may be called a bulk spin-flop (BSF) state which becomes increasingly ferromagnetic (F). No transition to a pure F state occurs at any finite field H. Since a cyclic chain preserves translation invariance, and thus provides a faithful representation of the bulk limit, we have in effect described the BSF transition on an infinite chain. The additional structure shown to the left of the boundary H_b in the phase diagram of Fig. 2 is due to surface effects that are analyzed in Sec. IV.

IV. SURFACE SPIN-FLOP TRANSITION

The numerical calculation described in Sec. III was subsequently repeated on an open chain with the same size $\Lambda = 10$, and the result is depicted by a solid line in Fig. 3. The magnetization is now seen to exhibit a sudden jump at a new critical field $H_s = 0.609\,225\,70$ which is in excellent agreement with Eq. (2.14) applied for $\Delta = 1.5$. This result is consistent with the theoretical development of Sec. II which predicts that the one-magnon surface mode becomes the ground state beyond H_s. One may then use the analytical results obtained on a semi-infinite chain to actually predict the magnetization, at least for some nontrivial field region above H_s.

The ground-state total magnetization again vanishes for $H < H_s$ but is equal to

$$M = \sum_{l=1}^{\Lambda} M_l, \quad M_l = (-1)^l \frac{\langle \psi_1 | T_l^z | \psi_1 \rangle}{\langle \psi_1 | \psi_1 \rangle} \tag{4.1}$$

for $H > H_s$ where $|\psi_1\rangle$ is now the state of the surface mode in the lower gap of Fig. 1. Therefore, the norm of this state is given by

$$\langle \psi_1 | \psi_1 \rangle = \sum_{n=1}^{\infty} (|A_n|^2 + |B_n|^2) = [1 + (\Delta - 2H - 2E_1)^2] \frac{\xi_1^2}{1 - \xi_1^2}, \tag{4.2}$$

where A_n and B_n are taken from Eq. (2.9) applied for $\xi = \xi_1$ and $E = E_1$ given by Eq. (2.11). Accordingly the local magnetization M_l is given by

$$M_{2n-1} = \frac{|A_n|^2}{\langle \psi_1 | \psi_1 \rangle} - \frac{1}{2}, \quad M_{2n} = \frac{1}{2} - \frac{|B_n|^2}{\langle \psi_1 | \psi_1 \rangle} \tag{4.3}$$

for odd and even sites, respectively, and the total magnetization by

$$M = \frac{1-(\Delta - 2H - 2E_1)^2}{1+(\Delta - 2H - 2E_1)^2}. \tag{4.4}$$

It should be clear that the preceding results are valid also for $H < H_s$ where the surface mode is not the ground state. In particular,

$$M(H=0) = \frac{\Delta^2 - 1}{\Delta^2 + 1} \tag{4.5}$$

is the total magnetization of the one-magnon surface state at vanishing field. At the critical field H_s, where $E_1 = 0$, Eq. (4.4) yields

$$M(H=H_s) = \frac{1-(\Delta - 2H_s)^2}{1+(\Delta - 2H_s)^2}, \tag{4.6}$$

which agrees with the jump observed at H_s in Fig. 3 to eight significant figures; as expected on the basis of our discussion of the size dependence of the surface modes in Sec. II.

Such an excellent agreement of the analytical prediction (4.4) with the finite-size results of Fig. 3 persists over a nontrivial field region $H_s < H < H_w$, as demonstrated in the inset which focuses on the first step of the main figure. Clearly a new transition takes place at H_w and the one-magnon surface mode ceases to be the ground state for $H > H_w$. One would think that the SSF transition proceeds beyond H_s by a cascade of level crossings induced by multimagnon surface modes. But the results of Fig. 3 clearly indicate that there exists only one additional crossing at the critical field $H_w \approx 1.06 < H_b$ for $\Delta = 1.5$.

In order to appreciate the precise nature of the transition at H_w we have examined the evolution of the *local* magnetization M_l with increasing bias field. Results for $\Delta = 1.5$ and $\Lambda = 10$ are shown in Fig. 4 for a selected set of field values, using a more or less obvious notation. We begin with the first Néel state $|N_A\rangle$ of Eq. (1.4) whose local magnetization is depicted in the $H = 0$ entry of Fig. 4. The Néel state persists as the absolute ground state until the field crosses the critical value $H_s = 0.609$ of Eq. (2.14). Just above H_s a surface magnon is realized in the ground state, as shown in the $H = 0.61$ entry which may be reproduced to great precision using the analytical prediction (4.3) obtained on a semi-infinite chain. With further increase of the applied field the surface magnon slowly approaches a boundary Ising domain wall of the type *uududu* . . . . However, a sudden change occurs at the critical field $H_w \approx 1.06$, as demonstrated in the $H = 1.07$ entry where a bulk domain wall appears at the center of the chain. This state is a slightly depleted version of an ideal Ising domain wall of the type . . . *uduudu* . . . , thanks in part to the finite value of Δ and to the applied field. The tendency for inflation of the domain wall with increasing field becomes apparent in the $H = 1.12$ entry, where the field was chosen to be slightly greater than the bulk critical value $H_b = 1.118$ of Eq. (2.7). It should be noted here that the anticipated BSF transition is replaced on an open chain by a rapid but rounded crossover which becomes increasingly sharp with increasing chain size. The inflation of the domain wall is more rampant at higher field values and the local magnetization approaches a nearly uniform ferromagnetic configuration within the bulk, with some nonuniformity persisting near the edges of the open chain; as is completely apparent in the last, $H = 2$, entry of Fig. 4. However, complete ferromagnetic order is achieved only when $H \to \infty$.

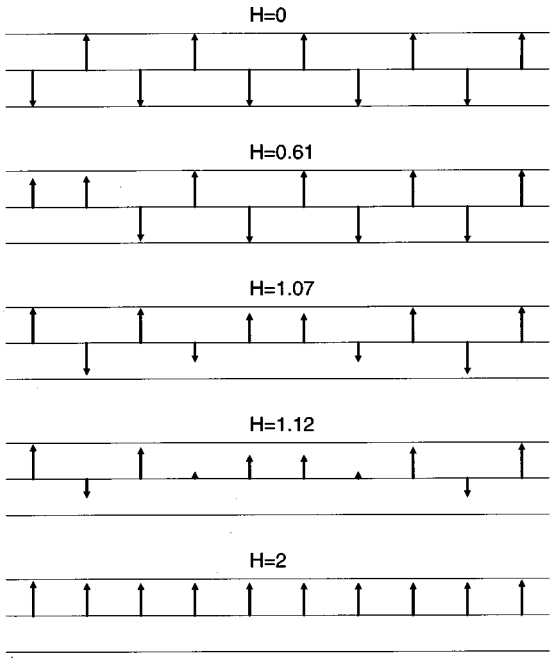

FIG. 4. Snapshots of the local magnetization M_l on a chain with $\Delta = 1.5$ and $\Lambda = 10$, for a characteristic set of field values described in the text.

The picture was completed with a detailed examination of the pertinent level crossings. Thus we calculated the ground-state energies of all sectors ($\tau = N, N-1, \ldots, -N$) as functions of the applied field H at the given anisotropy $\Delta = 1.5$. The first transition occurs at the critical field H_s where the Néel state $|N_A\rangle$, with $\tau = N$, is crossed by the one-magnon surface mode, with $\tau = N-1$. For higher fields, multiple level crossing take place among the lowest-energy states of the multimagnon sectors $\tau = N-2, N-3, \ldots$, and are likely to play an important role in the low-temperature dynamics. But most of these crossings are irrelevant for the determination of the absolute ground state because the one-magnon surface mode is eventually overtaken only by the ground state of the $\tau = 0$ sector which is an antiferromagnetic domain wall located at the center of the open chain.

The last remark prompted us to examine the local magnetization in the lowest-energy states of all sectors, even though most of these states do not become the absolute ground state for any field value. The result for $\Lambda = 2N = 10$ is presented in Table I using a symbolic notation that is strictly appropriate only in the extreme Ising limit $\Delta \to \infty$. But the essence of the derived picture at finite Δ and $0 < H \lesssim H_b$ is well represented in Table I. Thus the ground state in each

TABLE I. Symbolic illustration of the ground state in each sector on an open chain with $\Lambda=10$.

τ	Pseudospin	Spin	M
5	*uuuuuuuuuu*	*dududududu*	0
4	*duuuuuuuuu*	*ududududu*	1
3	*dduuuuuuuu*	*uddudududu*	0
2	*ddduuuuuuu*	*uduudududu*	1
1	*dddduuuuuu*	*ududdududu*	0
0	*ddddduuuuu*	*ududuududu*	1
−1	*dddddduuuu*	*udududdudu*	0
−2	*ddddddduuu*	*ududuuudu*	1
−3	*dddddddduu*	*ududududdu*	0
−4	*ddddddddu*	*udududuuu*	1
−5	*ddddddddd*	*udududududu*	0

sector ranges between the two pure Néel states of Eq. (1.4) which correspond to the two extreme values of the azimuthal pseudospin $\tau=\pm N$. For intermediate values of $\tau=N-\lambda$, with $\lambda=1,2,\ldots,2N-1$, a domain wall is formed at a distance equal to λ lattice units from the left boundary of the chain. Therefore, the good quantum number τ provides a rigorous definition of the relative location of a domain wall on an open chain, even at finite Δ where the wall expands and thus departs from its ideal Ising shape. Domain walls with opposite pseudospin $\pm\tau$ are displayed symmetrically about the center and carry the same energy. The least-energy state for $H>H_w$ is a $\tau=0$ domain wall located at the center of the chain.

To rule out the possibility of an accident that might have occurred for the specific size $\Lambda=10$ used so far, we repeated the calculation for $\Lambda=12$ and the results for the total magnetization are shown in Fig. 5. Surprisingly, two instead of one additional level crossings may now be discerned: the first at $H_w\approx1.06$, which is virtually identical to the value obtained earlier for $\Lambda=10$, and the second at $H_w'\approx1.09$ which indicates the existence of yet another critical field. This interesting twist in the general picture is clarified by the

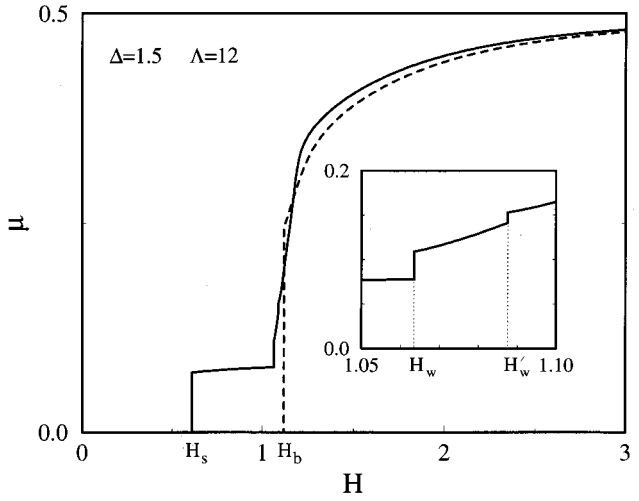

FIG. 5. Same as Fig. 3 for a chain with $\Lambda=12$. The inset now focuses on a narrow region near the critical field H_w to reveal the existence of a secondary critical field H_w'.

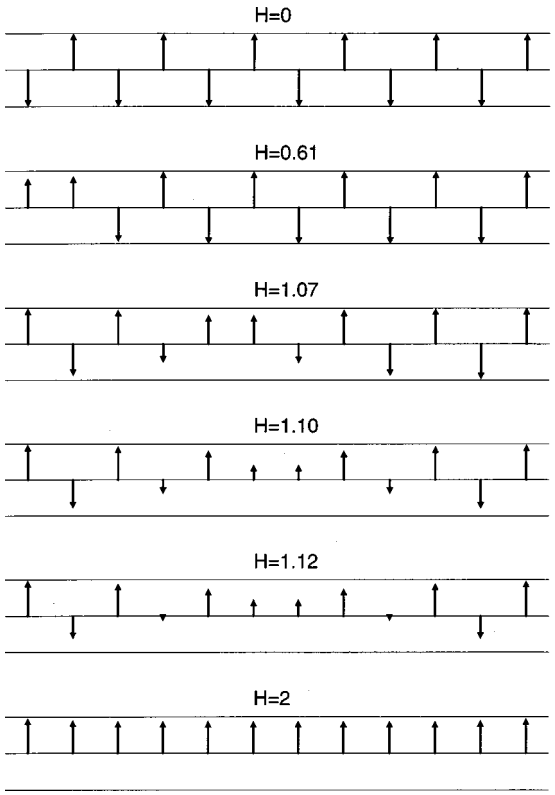

FIG. 6. Snapshots of the local magnetization M_l on a chain with $\Delta=1.5$ and $\Lambda=12$, for a characteristic set of field values described in the text.

results of the local magnetization M_l given in Fig. 6, in conjunction with an obvious extension of Table I to $\Lambda=12$.

At this point it is useful to address the last column of Table I which quotes the possible values of the total magnetization of domain walls in the extreme Ising limit, $M=0$ or 1. One may say that the two values correspond to domain walls of *dd* or *uu* type, respectively. Although these values are significantly modified at finite Δ, they nevertheless suggest that a level crossing is more likely to be induced by a *uu* state whose (negative) Zeeman energy in a (positive) field H is greater in absolute value. The $\tau=0$ domain wall at the center of the $\Lambda=10$ chain is indeed a *uu* state. However, when Table I is extended to $\Lambda=2N=12$, where $N=6$ is even, the $\tau=0$ domain wall becomes a *dd* state, whereas *uu* domain walls that are closest to the center are those with $\tau=\pm1$ and are likely to be energetically favorable.

Simple comparison of the $H=1.07$ entries in Figs. 4 and 6 reveals that the same domain wall of the *uu* type appears in both cases, but the wall in the second case is displaced by one lattice unit from the center of the chain. Since a bulk domain wall is rather narrow for the specific anisotropy $\Delta=1.5$ used so far, its energy is relatively insensitive to the precise location about the center even for short chains. This explains why the transition observed for $\Lambda=12$ occurs at virtually the same critical field $H_w\approx1.06$ found earlier for $\Lambda=10$, even though it now corresponds to a level crossing of the one-magnon mode by the ground state of the $\tau=1$ sector. However, the $\tau=0$ ground state, which originates in a *dd* domain wall at lower fields, ultimately becomes sufficiently frustrated to overtake the $\tau=1$ sector at a new critical field $H_w'\approx1.09$, as demonstrated by the $H=1.10$ entry of Fig. 6.

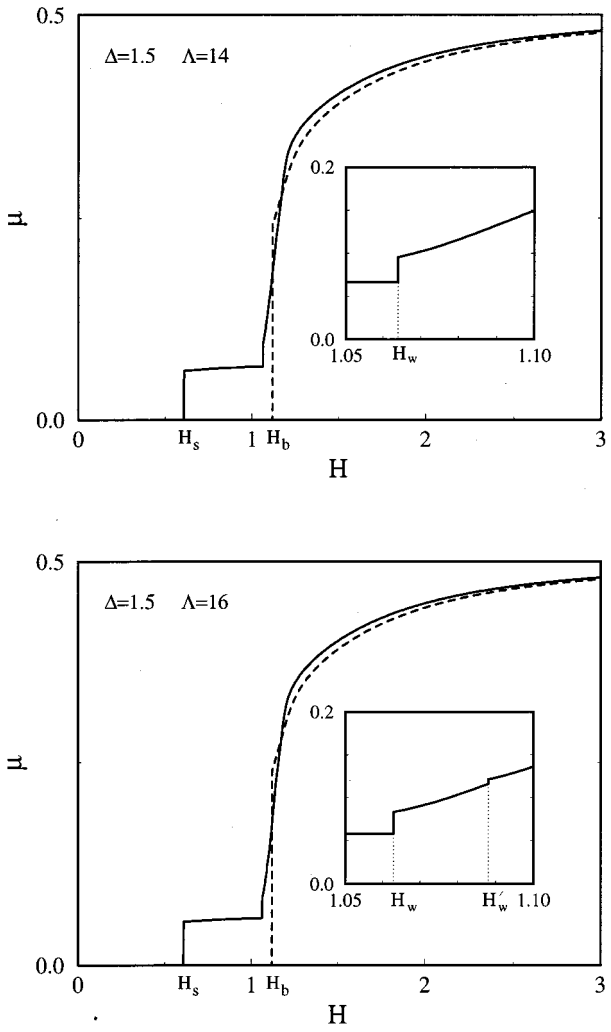

FIG. 7. The results of Figs. 3 and 5 now iterated on longer chains with $\Lambda=14$ and 16 to establish the alternating pattern described in the text.

The absolute ground state remains in the $\tau=0$ sector for $H>H'_w$ and is again rendered increasingly ferromagnetic in the limit $H\to\infty$.

The foregoing analysis suggests that a transition into a domain-wall state is always present on an open chain at a critical field H_w, and is merely decorated by a secondary transition at a slightly higher field H'_w when N in $\Lambda=2N$ is even. This alternating pattern is confirmed by the calculated total moment for $\Lambda=14$ and 16 shown in Fig. 7, and by further analysis of level crossings using the Lanczos algorithm on chains with $\Lambda\leqslant 22$. The main new critical field H_w quickly stabilizes to the size-independent value $H_w=1.0625$, for $\Delta=1.5$, which is distinct from the bulk critical field $H_b=1.118$ and thus clearly suggests the appearance of a definite domain-wall (DW) phase in $H_w<H<H_b$.

The picture just derived for the specific anisotropy $\Delta=1.5$ is more or less sustained for a wide range of anisotropies in the region $\Delta\gtrsim 1.25$. However, this simple picture becomes more involved as the anisotropy approaches the isotropic limit $\Delta\to 1^+$. Already at $\Delta=1.125$ a cascade of level crossings are induced by the least-energy states of the sectors $\tau=N-1,N-3,N-5,\ldots$ at a sequence of critical fields $H_s,H_w,H'_w,\ldots$ which stabilize to size-independent values. The main SSF transition is still given by the crossing of the $\tau=N$ Néel state by the $\tau=N-1$ surface magnon or boundary domain wall at the critical field H_s of Eq. (2.14). But the next transition at H_w now corresponds to a crossing of the $\tau=N-1$ surface magnon by the $\tau=N-3$ ground state which is a *uu*-type domain wall located three lattice units away from the left end of the chain. Subsequent transitions at a sequence of critical fields $H'_w,H''_w,\ldots$ correspond to a sequense of hoppings of the domain wall in steps of two lattice units until it arrives at the center of the chain. Once the domain wall reaches the center, its future evolution is similar to the one described earlier for $\Delta=1.5$.

A completely satisfactory description is not possible on the short chains used in the numerical calculations, because the size of the relevant domain walls increases to lattice dimensions in the limit $\Delta\to 1^+$. However, the observed pattern is sufficiently clear to provide unambiguous numerical evidence for the new critical boundary $H=H_w(\Delta)$ which completes the phase diagram of Fig. 2. Although this basic phase diagram does not reflect the fine structure in $H_w<H<H_b$ alluded to in the preceding paragraphs, it certainly contains all those elements that are likely to be important in practical applications.

Thus the ground state is purely Néel and the corresponding phase is labeled as antiferromagnetic (AF) for $H<H_s$. The region $H_s<H<H_w$ is characterized by a ground state which is a surface mode and is called a surface spin-flop (SSF) phase. The domain-wall (DW) phase extends in the region $H_w<H<H_b$ where a bulk domain wall is realized in the ground state. Finally the region $H>H_b$ corresponds to the bulk spin-flop (BSF) phase, studied in Sec. III, which becomes increasingly ferromagnetic (F). This explains the composite designation (BSF, F) in Fig. 2. The union of the AF, SSF, and DW phases would become an extended AF phase in the absence of free boundaries.

The description of the phase diagram is completed with a comment on the thermodynamic limit. Although the critical boundaries reach size-independent values, for practically all $\Delta>1$, bulk quantities such as the average magnetization per site $\mu=M/\Lambda$ become relatively insignificant in the limit $\Lambda\to\infty$ for $H<H_b$. For example, in the SSF phase, the total magnetization M is given analytically by Eq. (4.4) and is of order unity. Therefore, the average moment μ decreases linearly with $1/\Lambda$, a fact that is progressively apparent in Figs. 3, 5, and 7 which depict results in the range $10\leqslant\Lambda\leqslant 16$. Nevertheless surface effects are always present on open even chains of any size and could be observed in a magnetic meterial that is sufficiently doped to produce a statistically significant number of such chains.

V. CONCLUSION

The main advantage of the bulk and surface spin-flop transitions studied in this paper is that they are induced by a *uniform* bias field which can be easily applied and tuned to any desired value. This situation should be contrasted with the case of *boundary* fields[23] that are generally difficult to implement, especially in doped materials where open magnetic chains are produced within the crystal in a random manner. It is thus conceivable that the current theoretical

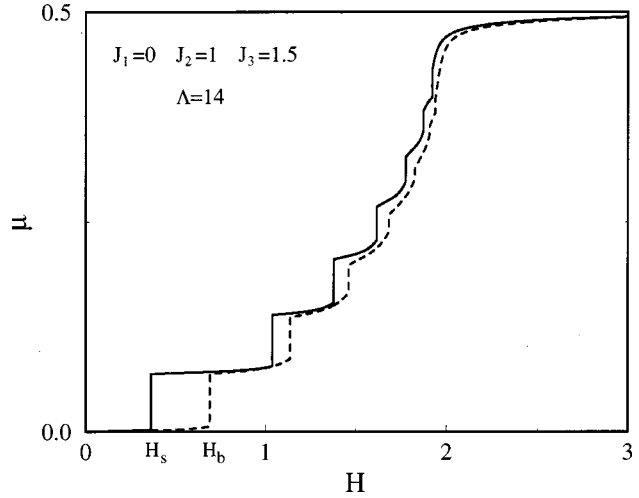

FIG. 8. Field dependence of the average magnetization per site $\mu = M/\Lambda$ in the ground state of a model with $J_1 = 0$, $J_2 = 1$, $J_3 = 1.5$, and $\Lambda = 14$. The dashed line corresponds to a cyclic chain and the solid line to an open chain with the same number of sites.

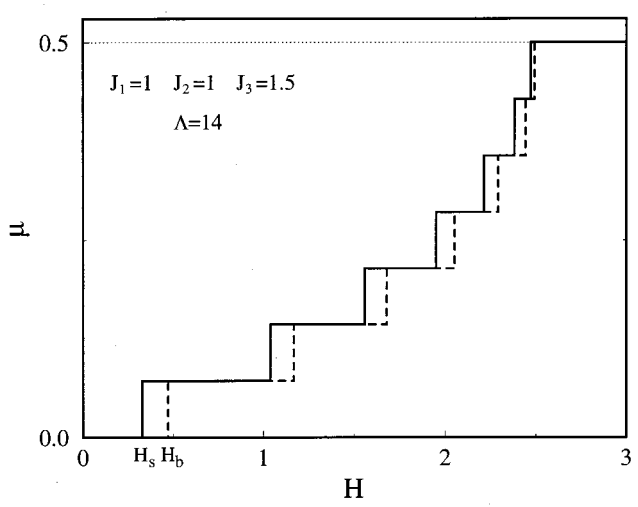

FIG. 9. Field dependence of the average magnetization per site $\mu = M/\Lambda$ in the ground state of the *XXZ* model $J_1 = 1 = J_2$, $J_3 = 1.5$ with $\Lambda = 14$. The dashed line corresponds to a cyclic chain and the solid line to an open chain with the same number of sites. Note the transition to a pure F phase above the critical field $H_f = 2.5$.

work will eventually find an experimental realization analogous to that obtained in classical Fe/Cr multilayers.[4–6]

Suppose that a quasi-one-dimensional magnetic material is found[22] with exchange constants that are approximately given by Eq. (1.3) after suitable normalization. Doping such a material with nonmagnetic ions[18] would produce open magnetic chains of varying size. Since the critical boundaries of Fig. 2 are practically independent of chain size, it would be possible to tune the applied field to the various regions of the phase diagram and thus probe the predicted magnetic phases. Electron-spin resonance at low temperature seems to be an appropriate experimental tool, in analogy with resonance experiments already performed[6] and theoretically discussed[6,17] for classical Fe/Cr multilayers. A corresponding study in the present quantum model would require explicit calculation of the relevant dynamic susceptibilities, an issue to which we hope to return in the future.

The prospects for experimental realization would be significantly enhanced if the present theoretical work could be extended to the full range of models defined by inequalities (1.2). For example, an interesting special case is the anisotropic *XY* model ($J_1 = 0$, $J_2 = 1$, $J_3 = \Delta > 1$), or *YZ* model in current notation, in the presence of an in-plane field applied along the easy axis. Analytical solution of this model does not seem possible at nonvanishing field, and theoretical analysis is further complicated by the lack of a U(1) symmetry. A preliminary numerical calculation of the ground-state total magnetization on a chain with $\Lambda = 14$ is shown in Fig. 8. While a trace of both a surface (H_s) and a bulk (H_b) critical field is again present, the spin-flop transition obviously proceeds by multiple level crossings which are difficult to study in detail by numerical simulations on short chains. A notable feature of Fig. 8 is that ferromagnetic order at high fields is now more robust.

The picture could again simplify in the *XXZ* model ($J_1 = 1 = J_2$, $J_3 = \Delta > 1$) where a U(1) symmetry is restored. The effect of a uniform field pointing along the symmetry axis is simply a linear Zeeman shift of the zero-field energy eigenvalues. The latter may, in principle, be obtained by the Bethe ansatz[19] known to apply to both a cyclic and an open chain,[26] and the problem of spin-flop transitions amounts to studying the density of level crossings induced by the linear Zeeman shift. In fact, the $T = 0$ phase diagram on an infinite chain was studied by Johnson and McCoy[27] and consists of an AF phase for $H < H_b$, a BSF phase for $H_b < H < H_f$, and a pure F phase for $H > H_f$. If we set $\Delta \equiv \cosh \Phi$ the critical field H_b is given by[28]

$$H_b = \sinh \Phi \sum_{n=-\infty}^{\infty} \frac{(-1)^n}{\cosh n\Phi}$$

$$= \sinh \Phi \frac{\pi}{\Phi} \sum_{n=-\infty}^{\infty} \frac{1}{\cosh\left[\dfrac{(2n+1)\pi^2}{2\Phi}\right]}, \qquad (5.1)$$

which differs significantly from Eq. (2.7) especially at weak anisotropies ($\Delta \to 1^+$ or $\Phi \to 0$) where the field (5.1) vanishes exponentially. Furthermore, a transition to a pure F state now takes place above the critical field

$$H_f = \Delta + 1. \qquad (5.2)$$

Comparison of the results for the total magnetization computed numerically on an open and a cyclic chain with $\Lambda = 14$, shown in Fig. 9, again suggests a SSF transition at a new critical field $H_s < H_b$. However, both H_b and H_s are now size dependent and hence the results of Fig. 9 are not sufficient to establish the existence of a SSF transition. Extrapolation of the relevant magnon gaps calculated on chains with $\Lambda \leqslant 22$ indicates a ratio H_b/H_s that remains remarkably close to its Ising value 2 for a wide range of strong anisotropies in the region $\Delta > 2$. Nevertheless extrapolation becomes problematic at weak anisotropies and thus a definite prediction near the isotropic limit is difficult to obtain numerically. It should be mentioned that a considerable amount of work has been devoted to the study of the *XXZ* model in the pres-

ence of boundary fields,[29,30] but the more direct questions raised here in the presence of a uniform bulk field do not seem to have been addressed.

To conclude, we note that interesting variations of the main picture may occur for various $|J_1| \leqslant J_2 < J_3$. In this respect, we recall that the classical[21] ground state is independent of J_1 and thus combines features of the entire class of quantum models in the above range. Therefore, although the earlier classical calculations for single-ion[14] and exchange[21] anisotropy provided extremely valuable motivation for the present work, their detailed results cannot be readily applied to the study of the respective quantum models.

ACKNOWLEDGMENT

We are grateful to Xenophon Zotos for assistance in the development of the Lanczos algorithm.

APPENDIX: THE ODD CHAIN

In a material that is randomly doped with nonmagnetic ions, approximately half of the produced open magnetic chains are composed of an odd number of sites ($\Lambda = 2N + 1$). It is thus important to also examine the ground state of odd chains in the presence of a bias field H. The two Néel states

$$|N_A\rangle = |d,u,d,u,\ldots,d,u,d\rangle,$$
$$|N_B\rangle = |u,d,u,d,\ldots,u,d,u\rangle \tag{A1}$$

are again mapped by Eq. (1.5) to two completely polarized ''ferromagnetic'' states which are exact eigenstates of the Hamiltonian (1.6) for any value of the applied field. However, degeneracy is now lifted by the bias field because the states (A1) carry nonvanishing total magnetization $M = \mp 1/2$ and the corresponding energy eigenvalues are given by $\pm H/2$. Therefore, when H is taken to be positive, $|N_B\rangle$ is the unique ground state with $M = 1/2$. Similarly, when H is negative, the unique ground state is $|N_A\rangle$ with $M = -1/2$. For definiteness, we assume that the bias field is positive, the case of H being completely analogous.

Our task is then to determine the critical field above which a spin-flop transition may take place. Examination of the one-magnon spectrum around the state $|N_B\rangle$ leads to a picture that is fairly similar to that of Fig. 1, with the following notable difference. The gap mode 1 is now missing from the spectrum, while mode $1'$ is duplicated. As a result there will be no SSF transition at the critical field H_s. Instead an odd open chain will proceed directly to a BSF transition which occurs by a cascade of successive level crossings in the vicinity of the critical field H_b. This picture is similar but not identical to the BSF transition on an even cyclic chain, studied in Sec. III, where all crossings take place at precisely the same critical field H_b. Putting it differently, the anticipated hidden symmetry of an even cyclic chain at the critical point is broken on an open chain.

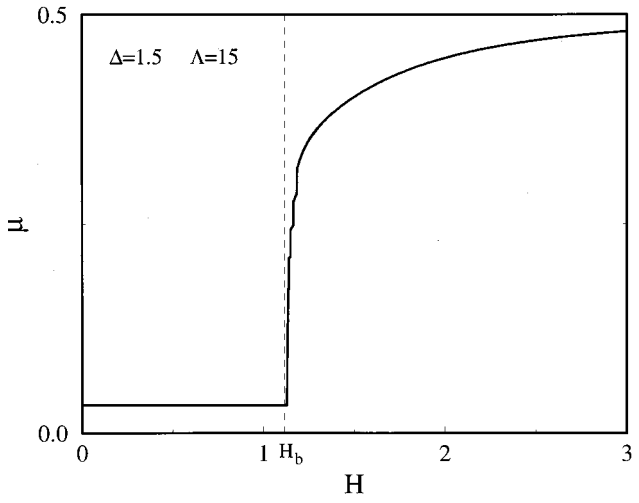

FIG. 10. Field dependence of the average magnetization per site $\mu = M/\Lambda$ in the ground state of our standard model (1.3) with $\Delta = 1.5$ on an open chain with an odd number of sites $\Lambda = 15$.

The lack of a SSF transition on an odd chain becomes apparent with an explicit calculation of the total magnetization for $\Delta = 1.5$ and $\Lambda = 15$ shown in Fig. 10. At low field values the total magnetization is given by $M = 1/2$, or $\mu = 1/2\Lambda$, and coincides with that of the pure Néel state $|N_B\rangle$. The BSF transition near the critical field H_b is also apparent in Fig. 10, whereas the chain is set on a more or less smooth course toward ferromagnetic order for $H > H_b$. Therefore, a clear distinction between even and odd chains is present, in analogy with the situation in classical Fe/Cr multilayers.[4,10]

*Electronic address: gkara@physics.uch.gr

†Electronic address: papanico@physics.uch.gr

[1] D. L. Mills, Phys. Rev. Lett. **20**, 18 (1968).

[2] D. L. Mills and W. Saslow, Phys. Rev. **171**, 488 (1968).

[3] F. Keffer and H. Chow, Phys. Rev. Lett. **31**, 1061 (1973).

[4] R. W. Wang, D. L. Mills, E. E. Fullerton, J. E. Mattson, and S. D. Bader, Phys. Rev. Lett. **72**, 920 (1994).

[5] R. W. Wang, D. L. Mills, E. E. Fullerton, S. Kumar, and M. Grimsditch, Phys. Rev. B **53**, 2627 (1996).

[6] S. Rakhmanova, D. L. Mills, and E. E. Fullerton, Phys. Rev. B **57**, 476 (1998).

[7] F. C. Nörtemann, R. L. Stamps, A. C. Carrico, and R. E. Camley, Phys. Rev. B **46**, 10 847 (1992).

[8] F. C. Nörtemann, R. L. Stamps, and R. E. Camley, Phys. Rev. B **47**, 11 910 (1993).

[9] R. L. Stamps, R. E. Camley, F. C. Nörtemann, and D. R. Tilley, Phys. Rev. B **48**, 15 740 (1993).

[10] R. W. Wang and D. L. Mills, Phys. Rev. B **50**, 3931 (1994).

[11] L. Trallori, P. Politi, A. Rettori, M. G. Pini, and J. Villain, Phys. Rev. Lett. **72**, 1925 (1994).

[12] L. Trallori, P. Politi, A. Rettori, M. G. Pini, and J. Villain, J. Phys.: Condens. Matter **7**, L451 (1995).

[13] L. Trallori, Phys. Rev. B **57**, 5923 (1998).

[14] C. Micheletti, R. B. Griffiths, and J. Yeomans, J. Phys. A **30**, L233 (1997).

[15] C. Micheletti, R. B. Griffiths, and J. Yeomans, Phys. Rev. B **59**, 6239 (1999).

[16] N. Papanicolaou, J. Phys.: Condens. Matter **10**, L131 (1998).

[17] N. Papanicolaou, J. Phys.: Condens. Matter **11**, 59 (1999).

[18] H. Asakawa, M. Matsuda, K. Minami, H. Yamazaki, and K. Kat-

sumata, Phys. Rev. B **57**, 8285 (1998).
[19] M. Gaudin, *La Fonction d'Onde de Bethe* (Masson, Paris, 1983).
[20] Zhan-Ning Hu, Phys. Lett. A **250**, 337 (1998).
[21] J. Karadamoglou and N. Papanicolaou, J. Phys. A **32**, 3275 (1999).
[22] J. Kyriakidis and D. Loss, Phys. Rev. B **58**, 5568 (1998).
[23] F. C. Alcaraz, S. R. Salinas, and W. F. Wrezinski, Phys. Rev. Lett. **75**, 930 (1995).
[24] H. P. Bader and R. Schilling, Phys. Rev. B **19**, 3556 (1979).
[25] V. Pasquier and H. Saleur, Nucl. Phys. B **330**, 523 (1990).
[26] F. C. Alcaraz, M. N. Barber, M. T. Batchelor, R. J. Baxter, and G. R. W. Quispel, J. Phys. A **20**, 6397 (1987).
[27] J. D. Johnson and B. M. McCoy, Phys. Rev. A **6**, 1613 (1972).
[28] J. D. Johnson and J. C. Bonner, Phys. Rev. B **22**, 251 (1980).
[29] M. Jimbo, R. Kedem, T. Kojima, H. Konno, and T. Miwa, Nucl. Phys. B **441**, 437 (1995).
[30] A. Kapustin and S. Skorik, J. Phys. A **29**, 1629 (1996).